



HAL
open science

Geodetic Matched Filter Slow Slip Event Detection Along the Northern Japan Subduction Zones

Lou Marill, David Marsan, Baptiste Rousset, Anne Socquet

► **To cite this version:**

Lou Marill, David Marsan, Baptiste Rousset, Anne Socquet. Geodetic Matched Filter Slow Slip Event Detection Along the Northern Japan Subduction Zones. *Journal of Geophysical Research: Solid Earth*, 2024, 129 (9), pp.e2024JB029342. 10.1029/2024JB029342 . hal-04780991

HAL Id: hal-04780991

<https://hal.science/hal-04780991v1>

Submitted on 13 Nov 2024

HAL is a multi-disciplinary open access archive for the deposit and dissemination of scientific research documents, whether they are published or not. The documents may come from teaching and research institutions in France or abroad, or from public or private research centers.

L'archive ouverte pluridisciplinaire **HAL**, est destinée au dépôt et à la diffusion de documents scientifiques de niveau recherche, publiés ou non, émanant des établissements d'enseignement et de recherche français ou étrangers, des laboratoires publics ou privés.

Geodetic Matched Filter Slow Slip Event Detection Along the Northern Japan Subduction Zones



Key Points:

- We search for slow slip events along the northern Japan subduction zones using a template matching approach on GNSS time series (1997–2020)
- We find 12 slow slip events on the Philippine Sea plate and 9 on the Pacific plate, coinciding with low locking areas
- A large gap devoid of any SSE correlates with the locked asperity of the 2011 M9 Tohoku-Oki earthquake

Supporting Information:

Supporting Information may be found in the online version of this article.

Correspondence to:

D. Marsan,
david.marsan@univ-smb.fr

Citation:

Marill, L., Marsan, D., Rousset, B., & Socquet, A. (2024). Geodetic matched filter slow slip event detection along the northern Japan subduction zones. *Journal of Geophysical Research: Solid Earth*, 129, e2024JB029342. <https://doi.org/10.1029/2024JB029342>

Received 17 APR 2024

Accepted 5 AUG 2024

Author Contributions:

Conceptualization: Lou Marill, David Marsan, Baptiste Rousset, Anne Socquet

Data curation: Lou Marill

Funding acquisition: Anne Socquet

Investigation: Lou Marill, Baptiste Rousset, Anne Socquet

Methodology: Lou Marill, David Marsan, Baptiste Rousset, Anne Socquet

Software: Lou Marill

Validation: Lou Marill

Writing – original draft: Lou Marill, David Marsan, Baptiste Rousset, Anne Socquet

Lou Marill¹ , David Marsan¹ , Baptiste Rousset² , and Anne Socquet¹ 

¹University Grenoble Alpes, University Savoie Mont Blanc, CNRS, IRD, University Gustave Eiffel, Grenoble, France,

²Institut Terre et Environnement de Strasbourg, Université de Strasbourg, CNRS, Strasbourg, France

Abstract We apply a template matching method on GNSS data for stations located in Honshu, Japan, to detect slow slip events associated with the subducting Philippine Sea and Pacific plates during the period from 1997 to 2020. A measure of the minimum detectable moment magnitude is proposed, from which we infer that the method could potentially detect SSEs as small as M_w 5.2 on the westernmost part of the Philippine Sea plate and M_w 6 on the Pacific plate below Honshu eastern coastline. We find 12 slow slip events on the Philippine Sea plate, among which eight are located on the known Boso slow slip event asperity and the four others are located offshore north-east relative to the Boso SSEs, at the transition with the Pacific plate. We find 9 SSEs on the Pacific plate, mainly on the northern section, offshore Iwate prefecture. A clear gap with no SSEs coincides with the main asperity that broke during the 2011 Tohoku earthquake. Most event locations correlate with low locking areas. We do not find any clear temporal pattern apart from the regular occurrence of the largest Boso SSEs.

Plain Language Summary Slow earthquakes are known to occur in northern Japan, especially off the Boso Peninsula. They are however harder to detect on the Pacific plate, likely due to their small sizes and/or their remoteness. We here apply a method that search for such slow ruptures, that process all the GNSS stations at once so to improve the signal-to-noise ratio. We find 21 such events, 13 of them being so far unrecognized. A clear lack of slow slip events is observed for the asperity that broke during the 2011 Tohoku-Oki earthquake. The absence of any regular pattern, outside the well-known Boso slow ruptures, is noticed, implying that the role of these events in the overall seismic cycle is still unclear for the Pacific plate subduction zone.

1. Introduction

With the development of Global Navigation Satellite System (GNSS) measurements in the 90s, systematic observations of transient slip events with low slip rate, either triggered by mainshocks (i.e., afterslip) (e.g., Heki et al., 1997; Peltzer et al., 1996) or with seemingly spontaneous onsets (i.e., Slow Slip Events (SSEs)) (e.g., Dragert et al., 2001; Lowry et al., 2001; Ozawa et al., 2001) have shown that fault slip is accommodated over a continuous, broad range of time scales (Peng & Gomberg, 2010). The importance of slow fault slip in the overall slip budget, and in the stressing of locked asperities, remains to be accurately evaluated, as only the largest slip events can be captured with GNSS recordings. Small SSEs are difficult to detect even for events releasing significant amount of slip (i.e., equivalent to M_w 5 to 6). Developing automated methods that allow to detect SSEs of smaller magnitudes (typically M_w 6 and below) (Costantino et al., 2023; El Yousfi et al., 2023; Frank et al., 2015, 2018; Kobayashi, 2017; Michel et al., 2019a; Nishimura et al., 2013; Okada et al., 2022; Rousset, Bürgmann, & Campillo, 2019; Rousset et al., 2017; Takagi et al., 2019) is important to characterize the properties of small SSEs, their scaling (Frank & Brodsky, 2019; Gomberg et al., 2016; Ide & Beroza, 2023; Ide et al., 2007; Michel et al., 2019b; Peng & Gomberg, 2010), and more generally to understand the frictional properties of faults.

Along the Japan trench, the Pacific (PAC) plate subducts below the North America plate at a rate of 76 mm/yr, and along the Sagami trough, the Philippine Sea (PHS) plate subducts also below the North America plate at a rate of 26 mm/yr while being on top of the PAC plate (Nishimura et al., 2007) (Figure 1). In these two subduction zones, observations of SSEs have been made, either directly from daily GNSS time series (Fukuda, 2018; Hirose et al., 2012; Ozawa et al., 2007, 2019), from tiltmeters (Hirose et al., 2012), from pressure gauges (Y. Ito et al., 2013), or more indirectly with observations of earthquake swarms (Gardonio et al., 2018; Kato et al., 2012), the latter only providing indirect evidence of the occurrence of transient slip.

The PHS plate is known to host recurrent SSEs offshore Boso peninsula (cyan circle in Figure 1a). From 1982 to 2022, 11 SSEs were detected directly using GNSS and tiltmeter time series (Fukuda, 2018; Hirose et al., 2012;

© 2024. The Author(s).

This is an open access article under the terms of the [Creative Commons Attribution-NonCommercial-NoDerivs License](https://creativecommons.org/licenses/by/4.0/), which permits use and distribution in any medium, provided the original work is properly cited, the use is non-commercial and no modifications or adaptations are made.

Writing – review & editing: Lou Marill,
David Marsan, Baptiste Rousset,
Anne Socquet

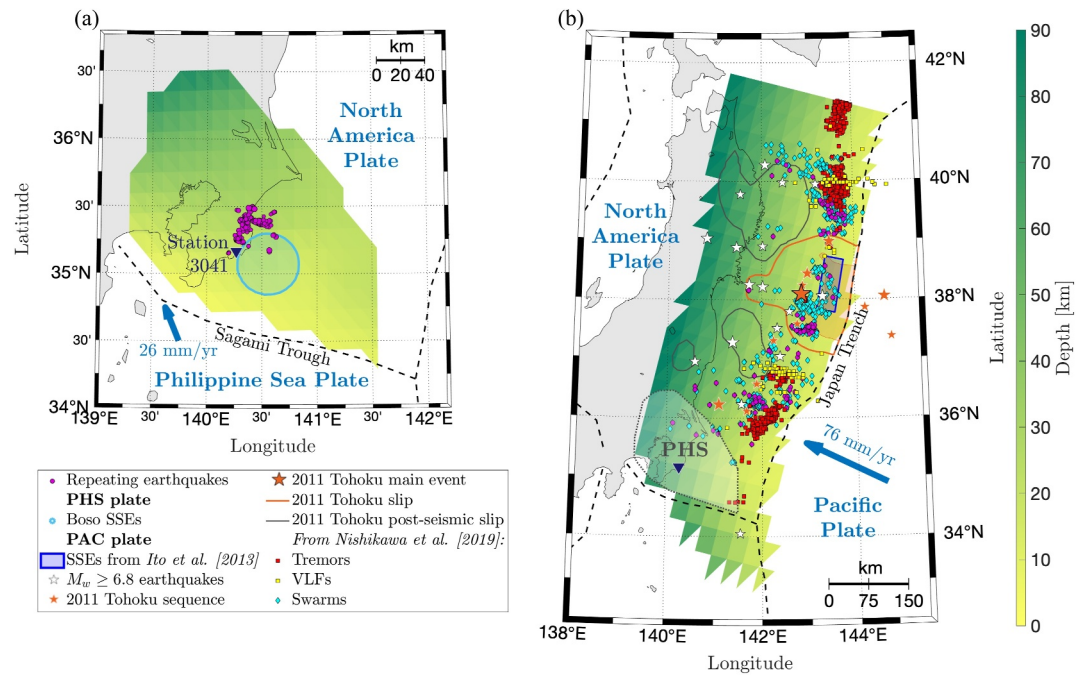


Figure 1. Seismo-tectonic setting of the Philippine Sea plate (a) and of the Pacific plate (b). Plate motions are deduced from Nishimura et al. (2007)'s Euler poles. (a) The colorbar gives the depth of the PHS plate (A. Ito et al., 2019; Uchida et al., 2010). The purple dots show repeating earthquakes from 2004 to 2016 (Gardonio et al., 2018). The cyan circle gives the location of the Boso SSEs (Nishimura, 2021). The blue triangle shows the station 3041 which time series is shown in Figure 2. (b) The colorbar shows the depth of the plate interface (Hayes et al., 2018). The dashed gray contour delimits the PHS plate (a). The purple dots show repeating earthquakes from 1997 to 2019 (Nishikawa et al., 2019). The red squares show tremors with a duration of at least 80 s from 2016 to 2019 (Nishikawa et al., 2019). The yellow squares present the Very Low Frequency Earthquakes from 2005 to 2019 (Nishikawa et al., 2019). The blue diamonds are swarm events from 1997 to 2019 (Nishikawa et al., 2019). The white stars show $M_w \geq 6.8$ earthquakes from 1997 to 2020. The orange star with black contour shows the M_w 9.0 2011 Tohoku earthquake. Other orange stars show $M_w \geq 6.8$ foreshocks and aftershocks of the Tohoku earthquake from 9 March 2011 to the 12 March 2011. The orange contour is the 40 m slip contour of the Tohoku-oki earthquake (Sun et al., 2014). The gray lines are the 0.5 m slip contours of the Tohoku earthquake afterslip 1 year after the earthquake (Sun et al., 2014). The blue rectangle shows the location of the SSE observed by Y. Ito et al. (2013) in 2008. The black dashed lines denote the plate boundaries.

Ozawa et al., 2007, 2019) and/or indirectly by analyzing seismicity or repeating earthquake sequences (Gardonio et al., 2018). The four first detected events occur ~ 6 years apart (1983, 1990, 1996 and 2002) (Hirose et al., 2012) while the following SSEs (2005, 2007, 2010, 2014, 2018) (Fukuda, 2018; Gardonio et al., 2018; Hirose et al., 2012; Ozawa et al., 2019) occur with a ~ 4 -year interval (Hirose et al., 2012; Ozawa et al., 2019). We did not consider the 2011 SSEs of March and October for the recurrence interval as they appear to be directly linked with the 2011 Tohoku earthquake. In average, these events are of M_w 6.5, with the minimum M_w in 2005 (M_w 5.8) (Gardonio et al., 2018; Ozawa et al., 2019) and the maximum M_w in October 2011 (M_w 6.7) (Fukuda, 2018; Ozawa et al., 2019). The duration of these SSEs ranges from 14 to 63 days (Fukuda, 2018; Ozawa et al., 2019). All the largest of these SSEs are accompanied by seismicity swarms at their bottom edges (Ozawa et al., 2019).

The PAC plate hosted the 2011 M_w 9.0 Tohoku megathrust earthquake (e.g., Hooper et al., 2013; Perfettini & Avouac, 2014; Sun et al., 2014). It ruptured a large part of the subduction interface, induced aftershocks down to the Kanto region and was followed by important afterslip with cumulative slip larger than 50 cm 1 year after the earthquake (Figure 1b) (Periollat et al., 2022; Sun et al., 2014). Afterslip was still going on at least for four more years (Sun & Wang, 2015). Before the Tohoku earthquake, the associated rupture area was almost fully locked, with a low locking zone on the northern edges of the rupture (Marill et al., 2021). A slow acceleration of slip in the decade that preceded Tohoku has also been identified (Hasegawa & Yoshida, 2015; Heki & Mitsui, 2013; Marill et al., 2021; Mavrommatis et al., 2014; Yokota & Koketsu, 2015). This acceleration is coherent with changes in repeating earthquake rates (Mavrommatis et al., 2015) and in background seismicity rates (Marill et al., 2021; Marsan et al., 2017). Within the area later ruptured by the Tohoku earthquake, Y. Ito

et al. (2013) found 2 SSEs using ocean-bottom pressure gauges and onshore strain-meters. Both events occurred just before an earthquake: in November 2008 a M_w 6.8 SSE lasting 14 days occurred before the December 2008 M_w 6.1 earthquake, and in February 2011 a M_w 7.0 SSE lasting 30 days occurred before the M_w 7.3 foreshock of the Tohoku earthquake (9 March 2011). Seismic evidences also point to the existence of aseismic processes at work in the weeks prior to the M_w 9 earthquake (Gardonio et al., 2019; Kato et al., 2012; Marsan et al., 2013). Even though slow slip on the PAC plate appears to contribute marginally to the overall slip budget dominated by megathrust earthquakes breaking a strongly locked asperity (Scholz & Campos, 2012), some of this activity likely played a role in clock-advancing the 2011 mainshock through direct stress transfer.

The PAC plate also hosts diverse seismic phenomenon associated to slow slip, including tremors, Very Low Frequency Earthquakes (VLFs), seismicity swarms and repeating earthquakes. Episodic tremor activity was discovered by Nishikawa et al. (2019) for the 2016–2018 period thanks to the analysis of the data from the S-net seafloor observatory (NIED S-net, 2019). The events are spatially segmented with no events in the area of the Tohoku earthquake rupture and swarms of events north and south of the rupture area (Figure 1). These two areas, corresponding to low locking areas (Marill et al., 2021), also host bursts of VLFs, seismicity swarms including M_w 5 to 6 events as well as repeating earthquakes. Also, the GNSS study of Nishimura (2021) in the Boso area suggests that 89 potential SSEs are actually located on the PAC plate, from 1994 to 2020. Those potential SSEs have $5.3 \leq M_w \leq 7.0$ and durations of up to 80 days.

In this study, we analyze the GNSS time series of 315 sites located on the Honshu Island in order to characterize short-term transient slip events. The GNSS time series are post-processed to correct for non-tectonic seasonal signals as well as co- and post-seismic displacements due to large earthquakes. In order to detect the transient slip events, we use the geodetic matched filter developed in Rousset et al. (2017) and apply it to the Sagami Trough and the Japan Trench. This method makes use of template matching between synthetic transient slip events computed from physics-based dislocation models and the post-processed GNSS time series. We perform an analysis of synthetic GNSS time series to characterize the lowest magnitudes of the transient events that can be detected with the method given a realistic noise amplitude before applying the method to the northern Japan subduction zones. Finally, we discuss our detections with respect to previous observations derived from both geodetic and seismological records.

2. GNSS Time Series

2.1. GNSS Data Processing and Time Series Analysis

We processed the raw data of the GNSS Earth Observation Network System (GEONET) of Japan using the version 1.2 of GipsyX (Bertiger et al., 2020) software, and loose No Net Rotation (NNR) orbits. To account for ocean tide loading, we use the FES2014b model (Lyard et al., 2021), using elastic Green function (Farrell, 1972), and with the Earth mass center correction provided by the Chalmers University of Technology (<http://holt.oso.chalmers.se/loading/>) as ocean tide loading model. The Vienna mapping function (Boehm et al., 2006) is used to estimate the tropospheric zenith delay parameters. No second order ionospheric correction is applied. Scaling, rotation and translation factors provided by the Jet Propulsion Laboratory are then applied in the Helmert transformation to map the loose NNR solution in the International Terrestrial Reference Frame (ITRF) ITRF2014 (Altamimi et al., 2017). Time series are available through Socquet et al. (2022).

We selected 315 stations in Honshu, located east of 139°E, and analyzed the period 1997–2020. To correct for known phenomenon other than possible SSEs impacting the time series—that is, antenna changes, co-seismic steps, post-seismic transients, seasonal variations and inter-seismic drift—we further developed the trajectory model of Marill et al. (2021) (ISTerre Time Series Analysis, ITSA). We model the post-seismic relaxation following the 2011 Tohoku earthquake with a sum of two logarithmic functions including different characteristic times (1 and 100 days) to account for both the early and longer term relaxations. The residuals from this analysis still contain long period non linear signals that are due to complexities in the post-seismic process not implemented in our simple model. In order to get rid of these years-long transient signal, we corrected the time series by subtracting a moving average with 4-year duration. At both ends of the times series, we avoid filtering edge effects by extending the time series with the same slope than the first and the last 2-year periods of the time series. We did not remove any already known SSEs, like the SSEs offshore Boso Peninsula (Fukuda, 2018; Ozawa

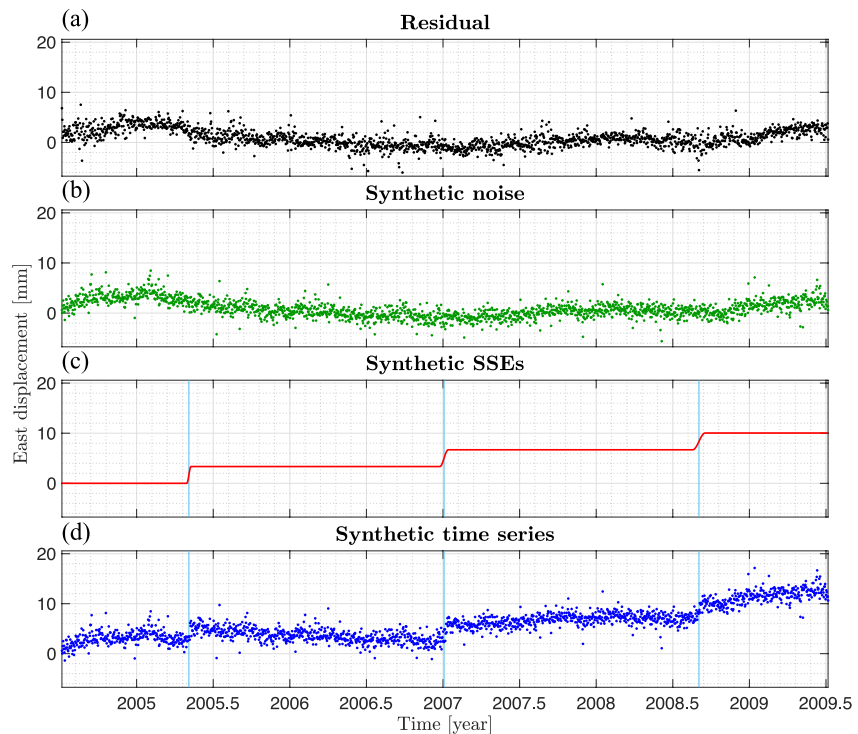


Figure 2. Generation of synthetic time series at station 3041 (blue triangle in Figure 1). (a) Residual time series obtained after the removal of the trajectory model from real data as explained in Section 2.1. (b) Synthetic noise obtained after the different steps explained in Section 2.2. (c) Synthetic displacement for three M_w 6.0 slow slip events with duration 10, 20 and 30 days respectively. (d) Synthetic time series obtained by summing the synthetic noise (panel b) and the synthetic displacement due to the transient slip events (panel c).

et al., 2019), since they are providing a benchmark test to validate the detection method for the largest events. We discarded the days for which less than half of the stations are active, and the 50 days after the Tohoku earthquake that are the most affected by mismodeling of the early post-seismic signal.

Large-scale common mode signals affecting the whole GNSS network can be due to orbital errors, issues in the reference frame realization, or large scale loading processes related to hydrology or ocean loading. In order to correct for common mode errors, we remove at each station the median of all the time series used in the study (Figure S1 in Supporting Information S1).

2.2. Synthetic Time Series

We created synthetic time series of noise to quantify the limits of the detection method and to characterize a detection threshold on real data. We followed the approach of Costantino et al. (2022) to construct realistic synthetic time series at each station based on the residual time series from the analysis described in the previous section. The synthetic time series are generated so that they keep similar spatial and temporal characteristics as the real ones. A Principal Component Analysis (PCA) is performed by taking into consideration all the stations of the network. The time series obtained by linear combinations with the PCA are then Fourier transformed, the phases are randomized, and are inverse Fourier transformed in the temporal domain. We then force the marginal distribution of each new time series to exactly match the marginal distribution of the PCA time series (Schreiber & Schmitz, 1996). An Inverse PCA is then applied, by multiplying each principal component with the corresponding transposed eigenvector, to get the final synthetic time series. The synthetic time series thus have the same (a) spatial covariance, (b) auto-correlation functions and (c) marginal distributions as the real ones. An example of synthetic noise is shown in Figure 2.

To generate synthetic time series, we then add to the noise time series the theoretical displacement induced by SSEs occurring either on the PHS or PAC plates, as predicted by the dislocation theory (Okada, 1985). To model

the PHS plate interface, we combined the interfaces of Uchida et al. (2010) for the part under the Kanto region and of A. Ito et al. (2019) for the offshore part. To model the PAC plate interface, we use the Slab 2 model (Hayes et al., 2018) from the Sagami Trough ($\sim 34.2^\circ\text{N}$) to the North of Honshu island ($\sim 41.3^\circ\text{N}$), and from the trench down to 90 km depth. The PHS plate is subdivided into 277 triangular patches and the PAC plate into 323 triangular patches. We defined the displacement templates for an SSE of unit slip that would occur on a patch i starting at time τ with surface displacement amplitudes G_{ij} (Green's functions), for all stations and horizontal components j , as:

$$\widehat{S}_j^{(i)}(t, \tau) = \begin{cases} 0 & \forall t < \tau \\ G_{ij} \times \left(-\frac{1}{2} \cos\left(\frac{t-\tau}{\Delta} \pi\right) + \frac{1}{2} \right) & \forall t \in [\tau; \tau + \Delta] \\ G_{ij} & \forall t > \tau + \Delta \end{cases} \quad (1)$$

Time τ corresponds to the start of the SSE, and Δ corresponds to the duration of the SSE. The symbol $\widehat{\cdot}$ is thereafter used to denote template (i.e., synthetic) quantities.

3. Template Matching Detection Method

3.1. Correlation and Detection

We then use the template matching detection method of Rousset et al. (2017). We first compute the correlation between the GNSS synthetic time series and the SSE displacement template. For each patch i , we select the stations for which a unit slip SSE on i would induce a theoretical displacement with a norm larger than 10^{-4} unit displacement at any given station. We then differentiate the template time series to obtain velocity templates $\widehat{V}_j^{(i)}(t, \tau)$, where j correspond to each station horizontal component. Velocity time series are more stable for the correlation than displacement time series due to the removal of linear trends in the displacement time series.

The correlation between the velocity templates $\widehat{V}_j^{(i)}(t, \tau)$ and the actual velocity time series $V_j(t)$ is then computed as:

$$C_{ij}(\tau) = \sum_t V_j(t) \times \widehat{V}_j^{(i)}(t, \tau) \quad (2)$$

The correlation is then normalized as:

$$\|C_{ij}(\tau)\| = \frac{C_{ij}(\tau)}{\sqrt{\sum_t V_j^2(t) \times \sum_t \widehat{V}_j^{(i)2}(t, \tau)}} \quad (3)$$

The total weighted correlation for patch i and at time τ is finally defined as:

$$C_i(\tau) = \frac{\sum_j |G_{ij}| \times \|C_{ij}(\tau)\|}{\sum_j |G_{ij}|} \quad (4)$$

where the sums are computed on all selected stations and horizontal components j .

We selected a template duration of 30 days. Such a duration allows us to detect transient slip events from 10 to 50 days, which correspond to the durations we are searching for. A detailed analysis of template durations and their influence on the analysis is described in Rousset et al. (2017). In Figure 3 is presented a synthetic correlation example with transient events of durations 10, 20 and 30 days. The associated correlation peaks (Figure 3c) have similar amplitudes well above the detection threshold, showing that the template duration does not impact the detection results much, for this range of durations.

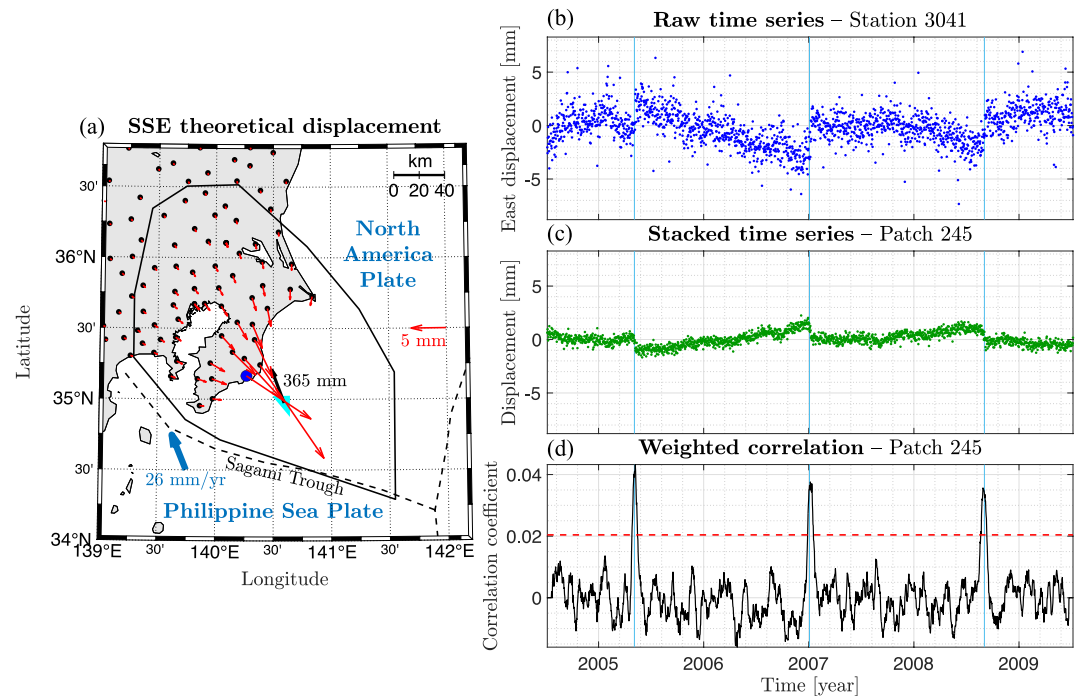


Figure 3. Illustration of SSE detection on three synthetic SSEs with duration 10, 20 and 30 days. (a) Synthetic displacement predicted by the dislocation theory for a M_w 6.0 SSE occurring on the light blue triangular patch of the PHS plate. (b) Synthetic time series at station 3041, shown by the blue dots on the left panel, obtained by summing synthetic noise and the synthetic displacements due to the slip events, (c) Stacked time series (Equation 5), (d) Total weighted correlation (Equation 4) showing correlation peaks at the times of the three synthetic SSEs. The red horizontal dashed line is the detection threshold at 8 times the MAD of the noise (MAD_n).

In order to detect transient slip events, we analyze the amplitude of the correlation functions to detect transient slip events. To establish a reliable detection threshold, we analyze synthetic time series composed of realistic noise and slip events on the subduction interface, for every patch. We vary slip amplitudes (and corresponding magnitudes) and detection thresholds, calculating the True Positive/All Positive (TP/AP) ratio after correlation analysis. This process is repeated 10 times for each parameter set, using various GNSS noise realizations, and we retain the median value. Figure S2 in Supporting Information S1 illustrates the results for a single patch located on the PHS plate subduction interface. Based on this analysis, we determined a maximum threshold of $8 \times MAD_n$ (Median Absolute Deviation on noise times series) on correlation functions without synthetic slip events ensures a TP/AP ratio of 1 across all subduction interface patches. We confirm the reliability of detections at this threshold by visually inspecting stacked GNSS time series for permanent static offsets at detection times. To adapt this threshold for correlation functions based on real GNSS time series, potentially including SSEs, we calculate the MAD_f (Median Absolute Deviation on full times series) and apply a scaling factor α to maintain the $8 \times MAD_n$ equivalence. The final detection threshold becomes $\alpha \times MAD_n$, with α computed separately for each patch.

With this definition of a detection threshold, we computed the minimum magnitude that can be detected on every location of the PAC and PHS subduction interfaces. Figure 4 shows that on the PAC plate, the minimum magnitudes that can be detected at the trench correspond to events with $M_w > 7$, while underneath Honshu the minimum magnitudes that can be detected are between 6 and 6.5. On the PHS interface, given the closer proximity of the GNSS stations to the slip interface, the minimum magnitudes that can be detected are $M_w \sim 6$ below the Boso peninsula and as low as M_w 5.2 at shallower depths.

For the detections on real data, we merge together successive detections if they occur less than 2 days apart, the final detection date then corresponds to the day of the largest correlation amplitude. The locations of the detected events are taken as the barycenter of the correlation, and we also indicate the 75% correlation amplitude contours as an estimation on the uncertainty on the location of the events (e.g., Figure 5). Finally, we validate the detections by visually inspecting the stacked GNSS time series defined as:

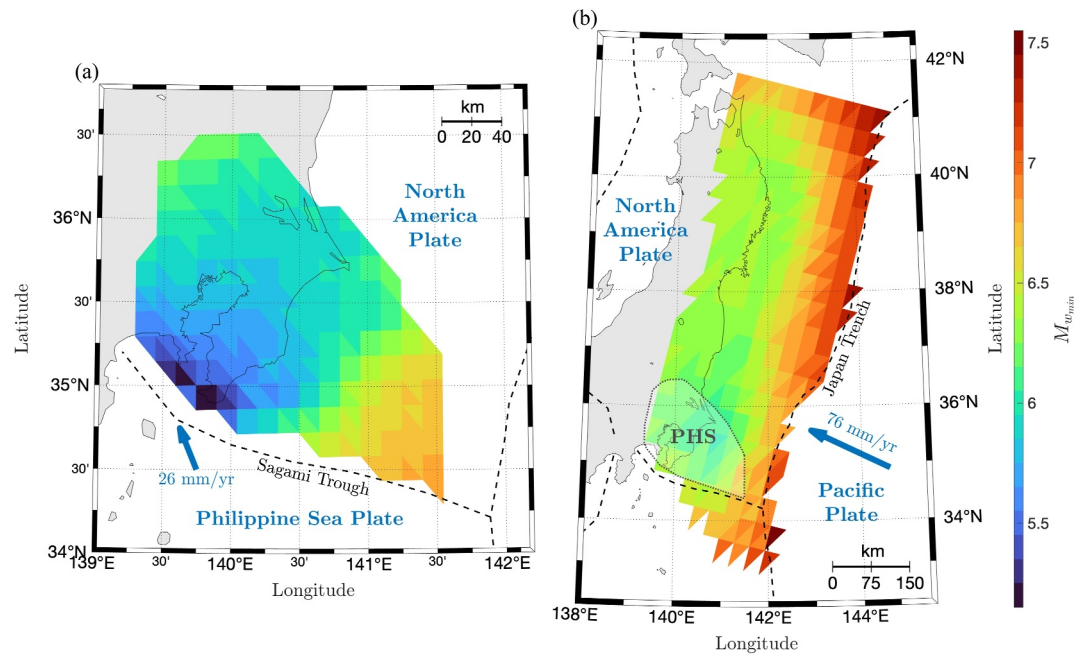


Figure 4. Estimated minimum M_w of transient slip events that can be detected for (a) the PHS plate and (b) the PAC plate.

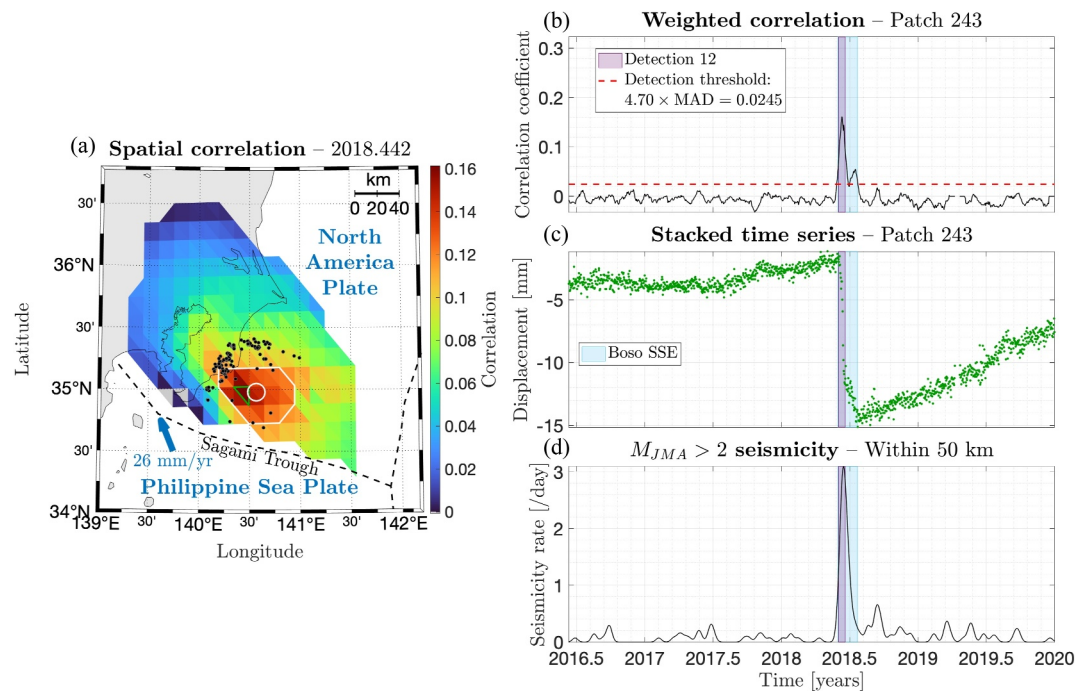


Figure 5. Example of detection for event 12 of the PHS plate, corresponding to the 2018 Boso SSE. The detection time is 2018.442, the estimated duration is 18 days and the estimated M_w is 6.7. (a) Amplitude of the correlation on the plate interface. The green triangle highlights the patch 243 with the larger correlation amplitude. The white line indicates the 75% contour, with the white circle corresponding to its barycenter. The black dots represent earthquakes within 50 km of the detection (used in panel (d)) (b) Time series of the correlation function. The dashed red line indicates the detection threshold. The purple rectangle shows the detected event. (c) GNSS weighted stacked time series. (d) Daily seismicity rate averaged over a 7-day time window from the $M_{JMA} > 2$ earthquakes within a radius of 50 km from the white circle.

$$S^{(i)}(t) = \frac{\sum_j G_{ij} S_j(t)}{|G_{ij}|} \quad (5)$$

where G_{ij} is the surface displacement amplitudes (Green's functions) at station j for an unit slip on patch i , and $S_j(t)$ is the displacement time series of the station j . A detection is validated as a transient slip event detection if we observe a permanent offset in the $S^{(i)}(t)$ time series.

3.2. Duration, and Moment Magnitude

To estimate the duration of the detected events, we model the stacked time series $S^{(i)}(t)$ associated with the patch of maximum correlation with a slow slip functional model, defined as:

$$\hat{S}(t) = s \left(-\frac{1}{2} \cos\left(\frac{t-\tau}{\Delta} \pi\right) + \frac{1}{2} \right) \quad (6)$$

which is similar to the template defined in Equation 1 except that the modeled duration Δ is variable. Parameter s corresponds to the amplitude of the observed offset in the stacked displacement time series. For a time window of length D days, centered on the detection time, we test different model durations Δ , from 2 to $D - 2$ days. We first find the best scaling factor s , that minimizes the Root-Mean Square Error (RMSE) between $S^{(i)}(t)$ and $\hat{S}(t)$. When computing the RMSE, we add more weight at the center of the time series by multiplying the difference between $S^{(i)}(t)$ and $\hat{S}(t)$ by a triangular-shaped function of duration D that has an amplitude of one at its center and zero at its edges. We then compare the RMSE values for all durations Δ and keep the Δ that minimizes the RMSE. As the length D of the window impacts the duration Δ obtained, we iterate this procedure for D from 10 to 60 days. If the best Δ ends at the edge of the time window D , we consider that a longer time window is needed to explain the time series (represented by black dashed lines in Figure S3 of Supporting Information S1, top right). The final estimated duration is the median of the kept Δ values. An example of duration estimation is shown in Figure S3 of Supporting Information S1 for 2018 detection in PHS.

We estimate the M_w of a given detection by fitting the amplitude of the static offset s on the stacked time series $S^{(i)}(t)$. The slip area A is taken as the area of the patch with the largest correlation amplitude, and we compute the slip value required so that the synthetic stacked offsets equal the amplitude observed in $S^{(i)}(t)$ (see Equation 5). The moment is then estimated with $M_o = \mu s A$ where the rigidity μ is 30 GPa. M_o is then converted into M_w (Hanks & Kanamori, 1979).

4. Distribution and Characteristics of the Detected SSEs

We first discuss the results for the PHS plate, starting with the Boso area, which allows us to compare our estimates (location, M_w , duration) with already published observations.

4.1. Known Boso SSE Asperity

We detect 8 SSEs on the known Boso SSEs asperity, among which the 5 largest are documented events: the 2002, 2007, October - November 2011, 2014 and 2018 Boso SSEs (Figure 6). A sixth Boso SSE is detected in April 2005 (event 4 in Table S1 of Supporting Information S1) with an estimated $M_w = 5.8$, that corresponds to the first SSE suggested by Gardonio et al. (2018) on the basis of a repeating earthquake analysis. The latter authors found two bursts of repeaters separated by ~ 1 month, and estimated the SSE M_w to be in the 5.8 to 5.9 interval. Our detection is coincident with the second burst. Similarly, a seventh Boso SSE is detected in 2009 (centered on the 18 December 2009) with an estimated $M_w = 6.2$ and a duration of 8 days, occurring close in time to the second suspected Boso SSE of Gardonio et al. (2018). The latter study evidenced a small burst of repeating earthquakes in the Boso area just following an increase in displacement rate along the N 40°E direction at the two closest GPS stations. We believe our detection indeed corresponds to this increase of repeating earthquakes, which occurred in late 2009. The estimated $M_w = 6.2$ matches with the one of Gardonio et al. (2018), who found $M_w = 6.1$. Finally, a

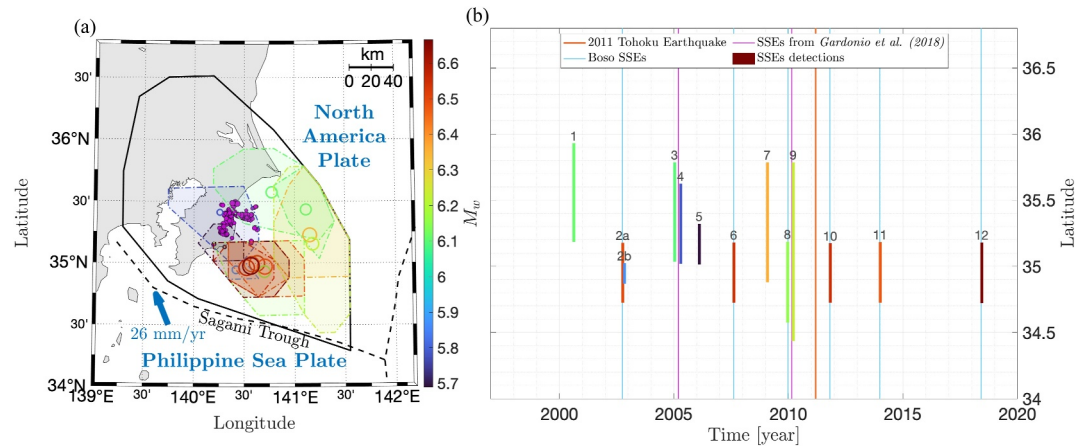


Figure 6. Detected SSEs on the Philippine Sea plate color-coded after their estimated M_w . (a) The circles show the barycenter of the detections and the colored areas contour the patches with a correlation larger than 75% of the maximum correlation. The black bold line represents the PHS plate contour. The purple dots show repeating earthquakes from 2004 to 2016 (Gardonio et al., 2018). (b) Detected SSEs in a latitude-time diagram. The length of the bars corresponds to the latitudinal extent of the 75% correlation amplitude. The orange vertical line marks the 2011 M_w 9.0 Tohoku earthquake occurrence time. The cyan vertical lines indicate the Boso SSEs in 2002, 2007, 2010, 2011, 2014, and 2018 (Fukuda, 2018; Ozawa et al., 2019), and the purple vertical bars are the small Boso SSEs detected in 2006 and 2010 by Gardonio et al. (2018).

eighth Boso SSE is found in February 2006 ($M_w = 5.7$, duration 14 days) that has not been documented elsewhere as far as we know. We checked that it did not trigger any occurrences of repeating earthquakes, considering the repeaters found by Gardonio et al. (2018).

In order to assess the quality of the method to find and characterize SSEs, we compare our results with already published characterizations of the seven largest Boso SSEs (i.e., all events but the February 2006 one). Table 1 gives the estimated moment magnitudes and durations, compared to those of Fukuda (2018), Gardonio et al. (2018) and Ozawa et al. (2019). The 2002 event correspond to two detections and is therefore described as composed of two sub-events separated by a time delay (Figure 6 and Figure S7 in Supporting Information S1). The durations obtained in our findings align well with previous studies, although duration estimates differ by 2–10 days. This variation is likely due to the emergent nature of SSEs, with slow beginnings and ends, making the duration estimates susceptible to change in the estimation procedure. Published durations often rely on single GNSS time series, while our stacked time series approach captures the entire SSE duration. This difference may explain slightly longer durations in our results, as stacked data account for variations across GNSS sites that might occur during SSE propagation.

These seven largest Boso SSEs (2002, 2005, 2007, 2009, 2011, 2014 and 2018) are also detected, when applying the detection analysis for the PAC plate, with centroids that are offset by about 50 km to the east compared to the expected location - with the exception of the M_w 5.9 2005 SSE, which is located on the PAC plate at about the same latitude and longitude as it is on the PHS plate. This spatial bias, along with the fact that the direction of the slip vector on the PAC plate is not optimized to explain slip on the PHS plate, explains the systematic offsets on the PAC-related M_w estimates, that are in the +0.2–+0.3 range, compared to the M_w estimates for the PHS plate. These are very clear cases of duplicate detections (i.e., simultaneous detections on both plates). Other possible cases of duplicate events have been systematically checked for. In case of a duplicate event, only one final detection is kept and attributed to the plate for which the final correlation amplitude is the greatest relative to the threshold level.

Table 1
Boso SSE Characteristics, Taken From (1) Fukuda (2018), (2) Gardonio et al. (2018) and (3) Ozawa et al. (2019), Compared to Our Study

Year	M_w	Duration (days)	Reference
2002	6.7	8 + (13) + 23	(1)
	6.7	14 + (8) + 24	this study
2005	5.8–5.9	1 month	(2)
	5.8	42	this study
2006	5.7	14	this study
2007	6.6	10	(1)
	6.5	18	this study
2009	6.1	10	(2)
	6.1	8	this study
2011	6.7	13	(1)
	6.6	18	this study
2014	6.6	12	(1)
	6.5	18	this study
2018	6.8	12	(3)
	6.7	18	this study

Note. The 2002 event is made of two sub-events, the duration in parentheses being the delay between the two sub-events.

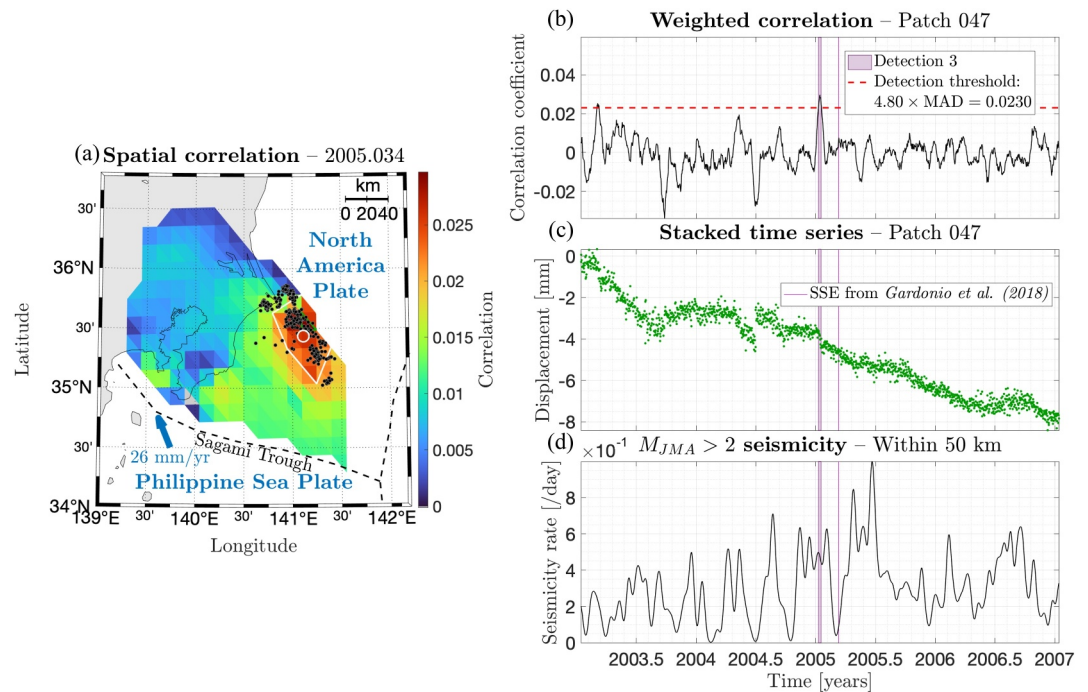


Figure 7. Same as Figure 5 but for event 3 detected on the PHS plate at time 2005.034, with estimated duration 18 days and estimated M_w of 6.1.

4.2. Rest of the PHS

On top of the eight Boso SSEs, four other events are found to the north-east, offshore Choshi in 2000, 2005 (Figure 7), 2009 and 2010. The spatial extent of the highest correlation amplitudes is larger than for the Boso detections due to a larger uncertainty on their locations, which is expected for offshore events of rather small magnitude (Figure 6). Those SSEs have estimated magnitudes ranging from 6.1 to 6.4, hence lower than the largest Boso events. This, along with the fact that their centroids are located typically 50–100 km more to the East, can explain why they have so far escaped detection in previous analyses. Their locations largely coincide with the swarm-prone area of Nishikawa and Ide (2017) (their Figure 3), and could also be related to the easternmost patch of SSEs of Nishimura (2021) along the Sagami Trough at about 141.5° of longitude (rectangle Sa2 on their Figure 7). By comparing our detections in time with the ones of Nishimura (2021) in Figure S4 of Supporting Information S1, we found that all the Boso SSEs with M_w 6.5+ match, as well as one event early 2006. However, most of the detections outside the Boso area did not coincide in time, neither with the probable SSEs found by Nishimura (2021) nor the swarms reported by Nishikawa and Ide (2017). We also checked whether the cumulative moments of these four SSEs would show an accelerating pattern over the detection period up to 2011, as could be expected given that this zone exhibits an acceleration of the seismicity rate from 1990 to 2011 (Marsan et al., 2017) (their Figures 6 and 7) as well as decreased locking (Marill et al., 2021). The rate of released moment by these four SSEs however appears steady from 2000 to 2011. No other SSEs are found in this zone after 2011, which could possibly be caused by an observational bias due to the 2011 Tohoku earthquake post-seismic phase being not perfectly modeled, that is, large residuals exist after 2011 that impact the correlation analysis.

Table S1 in Supporting Information S1 provides a list of the 12 PHS SSEs along with their characteristics. Figures S5–S15 in Supporting Information S1 show the 10 PHS SSEs distinct to the two shown in Figures 5 and 7.

4.3. SSE Activity on the Pacific Plate

Long-term changes in locking, at the scale of years to tens of years (Hasegawa & Yoshida, 2015; Heki & Mitsui, 2013; Loveless & Meade, 2016; Marill et al., 2021; Mavrommatis et al., 2014; Yokota & Koketsu, 2015) have been observed along the PAC plate before the 2011 Tohoku earthquake. However, short-period (at the scale of days to weeks) SSEs have so far escaped detection, apart from two events captured by ocean-bottom pressure

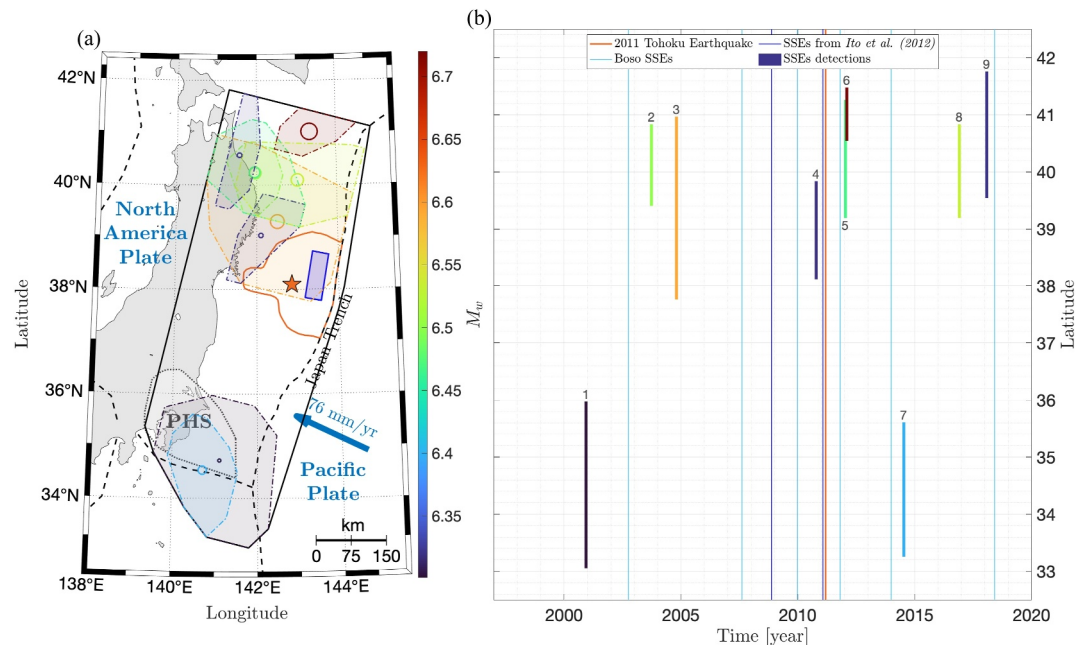


Figure 8. Detected SSEs on the Pacific plate color-coded after their estimated M_w and compared to known SSEs in the same area. (a) The circles (whose scale correspond to the M_w) show the best locations (barycenter) of the detections and the colored areas contour the patches with a correlation amplitude larger than 75% of the maximum correlation. The black bold line is the PAC plate contour and the black dashed line the PHS plate contour. The blue rectangle shows the location of the SSE observed by Y. Ito et al. (2013). The orange star with black contour shows the M_w 9.0 2011 Tohoku earthquake. The orange contour is the 40 m slip contour of the Tohoku earthquake (Sun et al., 2014). (b) Detected SSEs in a latitude-time diagram. The length of the bars corresponds to the latitudinal extent of the 75% correlation amplitude. The orange vertical line shows the 2011 M_w 9.0 Tohoku earthquake occurrence time. The cyan vertical lines indicate the Boso SSEs in 2002, 2007, 2010, 2011, 2014, and 2018 (Fukuda, 2018; Ozawa et al., 2019), and the blue vertical lines are the two SSEs detected by Y. Ito et al. (2013) in 2008 and 2011.

gauges (Y. Ito et al., 2013) and possible detections from Nishikawa and Ide (2017) close to the PHS plate. There are however strong hints that suggest the possible—if not likely—existence of other SSEs in the northern Japan subduction zone. Such hints include (a) clusters of repeating earthquakes that would be caused by sudden increases of slip rate along the subduction interface (Uchida et al., 2016), (b) swarm-like seismicity behavior (Imanishi et al., 2012; Marsan et al., 2013), (c) seismicity migration patterns, as for example, observed prior to the 2011 mainshock (Kato et al., 2012), (d) intermittency of the creep rate computed from spatial gradients of GNSS velocities along trench-normal profiles, which does not however allow to resolve spatially slow slip locations (Khoshmanesh et al., 2020), and (e) the existence of slow earthquakes (VLFs and tremors) captured by the seafloor observatory (Nishikawa et al., 2019).

Applying the geodetic matched filter, we detect 9 SSEs on the PAC slip interface, with M_w ranging from 6.3 to 6.7 (see Figure 8 and Table S2 in Supporting Information S1). Two SSEs occurred in close succession (time gap of 20 days) in January and February 2012 at latitudes 39°–41°, and could possibly be two sub-events of a larger and longer SSE affecting a wider slip area.

Like for the PHS plate SSEs found far offshore, the highest correlation footprints of those SSEs have large spatial extents (between 100 and 300 km wide), implying that their localization is largely uncertain. For 3 of them (the 2003, 2010, and 2018 SSEs), the depth is however relatively well resolved based on high correlation amplitudes, and points to slow slip occurring at 50–60 km depth, a depth range where slip at the plate boundary is expected to be mostly aseismic. It must be emphasized that SSEs in subduction zones tend to be shallower, ~40 km depth (Nishimura et al., 2013; Radiguet et al., 2012; Schmidt & Gao, 2010; Wallace & Beavan, 2010), and are sometimes located directly underneath locked segments. Deeper SSEs are found in the 40–60 km depth range in Chile (Klein et al., 2018), and in Alaska (Rousset, Fu, et al., 2019). We are not able to assign the other SSEs with

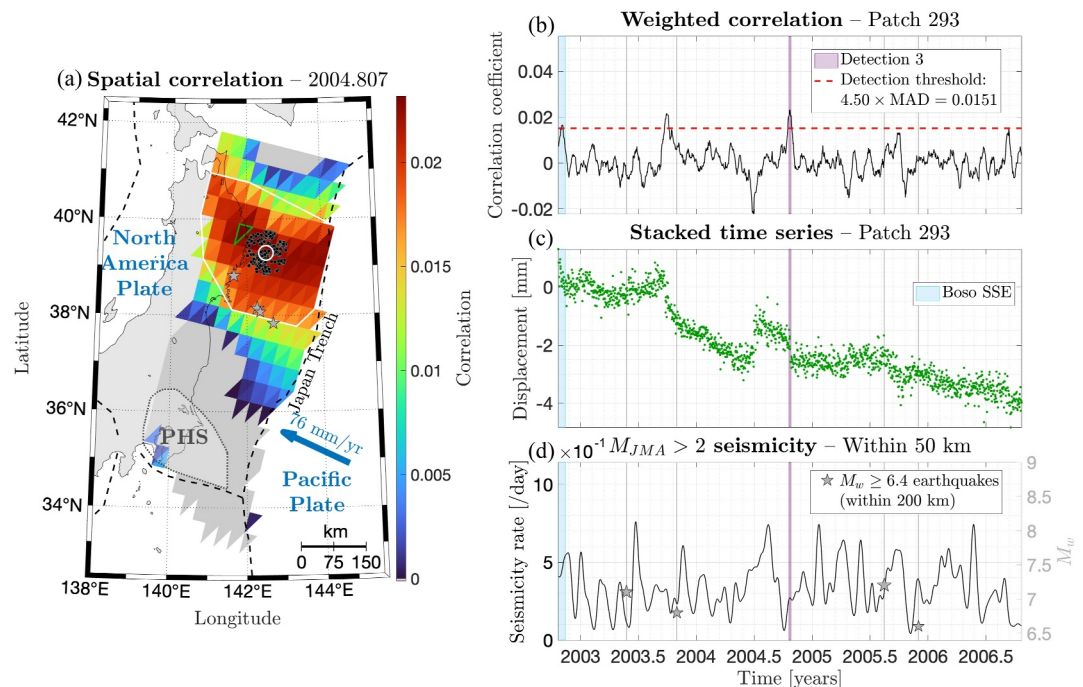


Figure 9. Same as Figure 5 but for event 3 detected on the PAC plate at time 2004.807, with estimated duration 38 days and estimated M_w of 6.5. The gray stars in (a) and (d) show the earthquake epicenters with $M_w \geq 6.4$ within a radius of 200 km from the white circle.

confidence to a specific depth nor distance to the trench: they could indeed be located in the mostly locked updip portion of the PAC, or downdip of it (down to about 60 km depth).

Among these nine events, seven are found in the northernmost part of the studied region (i.e., at latitudes greater than 38°), hence in coherence with the previously discussed hints suggesting that this zone is prone to slow slip processes. We show an example in Figure 9 (other events are shown in Figures S16–S23 of Supporting Information S1). The other two SSEs are found near the Sagami Trough, in 2000 and 2014. The gap between the two SSE-prone areas therefore extends from 35° to 38° of latitude. We note that this gap is documented by Nishikawa et al. (2019) as hosting tremor and Very Low Frequency earthquakes, but, according to our study, is thus devoid of M_w 6-class SSEs.

The two SSEs observed in the south ($35\text{--}36^\circ$ of latitude) are also detected when applying the detection algorithm on the PHS plate, but with a smaller correlation amplitude above the threshold. Their spatial extents overlap those seen for the SSEs on the PHS plate east of the Boso slipping patch, as described in Section 4.2. Since the two plates are in contact in this area, and since the depth and location is not well resolved as they are offshore, it cannot be excluded that those two events are additional instances of the 4 SSEs observed there on the PHS. Nishikawa et al. (2021) also found this area of the PHS plate to be prone to SSEs, even though we do not find as many events. Nishimura (2021) reports 25 probable and 64 possible SSEs with estimated M_w ranging from 5.6 to 6.9 along the Japan Trench at these latitudes, for the period 1994–2020, while we detected only two for 1997–2020.

Overall, the 9 SSEs on the PAC plate are found in areas with low locking (~ 0.3) (Figure 10a). The northern ones also coincide with the deceleration area before the Tohoku-oki earthquake (Figure 10b). The large gap between the northern and the southern SSE-prone areas corresponds to the asperity that broke in 2011. Some of the aseismically slip occurring in these low locking zones seems thus accommodated through episodic transients, although the cumulative moment released by these SSEs amounts to about 5.10^{19} N.m over 24 years, hence the equivalent of the yearly seismic moment rate of a $30 \times 30 \text{ km}^2$ patch on the PAC plate, which is small compared to the size of the low locking areas. Most of the aseismic slip is then accommodated either by smaller undetected SSEs or continuous aseismic slip.

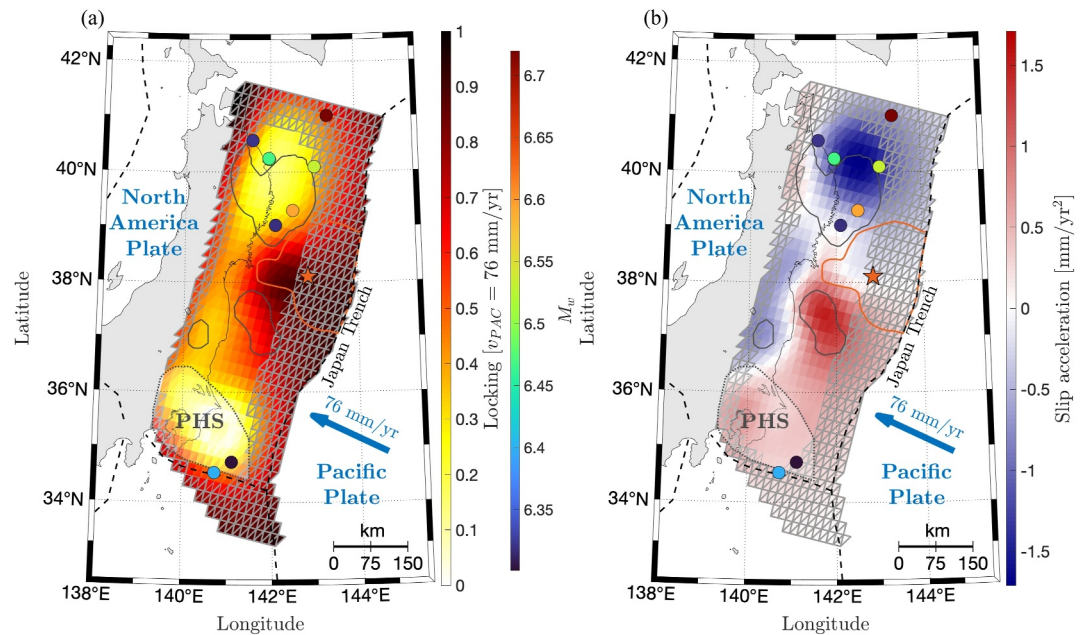


Figure 10. Pacific plate SSE locations found in this study compared to (a) the inter-seismic locking and (b) the 14-year slip acceleration before the 2011 Tohoku earthquake from Marill et al. (2021). The events are represented by colored circles, with the color indicating their magnitude according to the colorbar of Figure 8. The gray triangles correspond to the patches not resolved by inland GNSS data for the locking and slip acceleration. The gray contours, orange contours and orange stars are the same as in Figure 1.

We do not find any SSEs that would correspond to the two events reported by Y. Ito et al. (2013) based on ocean bottom pressure gauge and onshore strainmeter measurements. We paid specific attention to the correlation time series for the interface patches that hosted these events, as they could have missed the detection threshold by little. This is however not the case (Figures S24 and S25 in Supporting Information S1). We note that these SSEs have estimated M_w of 6.1 for 2008 and 7.3 for 2011 (Y. Ito et al., 2013). The 2008 SSE is thus effectively well below our detection limit of 6.5–6.6 here, but a more thorough investigation is needed to understand why the 2011 SSE is undetected.

4.4. Spatio-Temporal Patterns

There is no obvious temporal pattern in the SSE time series, see Figure 11. Only the largest, repeating Boso SSEs display some regularity, with a recurrence interval of ~ 4 years (Ozawa et al., 2019). For the deeper PHS and PAC plates events, the low spatial resolution does not permit us to infer the existence of other repeating slow slip as in Boso. The pseudo-periodic pattern of Boso SSEs thus appears as unique at the scale of the northern Japan subduction.

4.5. Seismicity Related to Detected SSEs

We computed the $M_{JMA} > 2$ earthquake rate time series within 50 km of each SSE centroid, as for example, displayed in Figure 5. The choice of this specific range (50 km) is based on the Boso SSEs, for which burst-like earthquake activity occurs on the down-dip portion of the fault, so to make sure that our selection does indeed encompass this activity. Apart from the five largest Boso SSEs, no other SSE is accompanied by a coincident burst of seismicity. Two smaller Boso SSEs were previously shown to be accompanied by repeating earthquake activity (Gardonio et al., 2018) but no significant increase in regular earthquake activity is seen for these two events. The

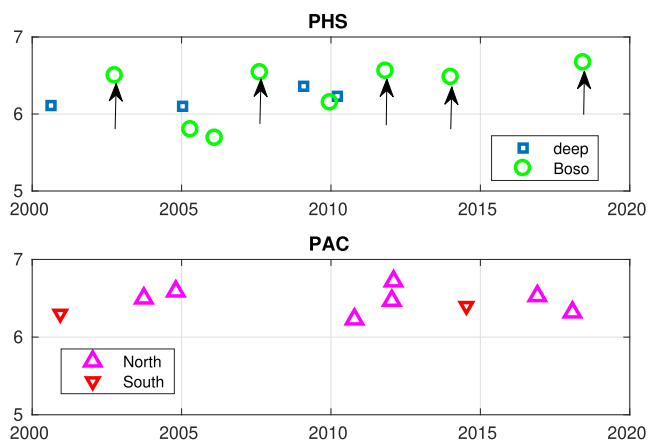


Figure 11. Magnitude versus time for the PHS and PAC SSEs. We distinguish the Boso and the deeper SSEs on PHS, and the North (latitude 38° and greater) and South (latitude 36° and less) groups of PAC SSEs. The arrows point to the SSEs that have a clear burst of seismicity (within 50 km) at the time of their occurrence.

fact that all other 16 SSEs (both on the PAC and PHS plates) have no clear coincident seismicity burst is likely due to two reasons: (a) most of these SSEs have smaller slip amplitudes and thus produced smaller associated Coulomb stress changes in their neighboring regions, and (b) they are all deeper, although, as mentioned previously, some PAC plate SSEs have an unresolved depth. Depth has been shown to be a first-order control on the number of earthquakes triggered by slow slip (Delahaye et al., 2009; Passarelli et al., 2021), which may explain the absence of burst-like seismicity for these deeper SSEs.

5. Conclusion

We applied a geodetic template matching method to the Sagami Trough and the Japan Trench in order to identify new small SSEs. From tests on synthetic time series we objectively determined a detection threshold for each patch of the PHS and PAC plates. We noticed that the limit magnitude of detectable SSEs depends on the depth of the patch and its distance to the GNSS stations; we determined that this detection threshold ranges between 5.2 and 6.8 (in M_w) for the PHS plate and 6 and 7.5 for the PAC plate. Applying our detection method to the real data, we found 12 SSEs on PHS, among which eight are located at the known Boso SSEs asperity, and 9 SSEs on PAC, mostly located in the northernmost part of our study area (latitude 38° and greater) but also with two instances near the Sagami Trough. All SSEs are located in areas of low interface locking (~0.3), but no clear link can be made with slow changes in locking at the time scales of years.

Data Availability Statement

All time series used in this manuscript and software are available at (Marill et al., 2024).

Acknowledgments

This work has been supported by the Agence Nationale de la Recherche (ANR-17-CE31-0002-01) AtypicSSE project and by ERC CoG 865963 DEEP-trigger project. We thank the Associate Editor (Yosuke Aoki) and two anonymous reviewers for their time, their constructive comments, and allowing us to improve our manuscript.

References

- Altamimi, Z., Métivier, L., Rebischung, P., Rouby, H., & Collilieux, X. (2017). ITRF2014 plate motion model. *Geophysical Journal International*, 209(3), 1906–1912. <https://doi.org/10.1093/gji/ggx136>
- Bertiger, W., Bar-Sever, Y., Dorsey, A., Haines, B., Harvey, N., Hemberger, D., et al. (2020). GipsyX/RTGx, a new tool set for space geodetic operations and research. *Advances in Space Research*, 66(3), 469–489. <https://doi.org/10.1016/j.asr.2020.04.015>
- Boehm, J., Niell, A., Tregoning, P., & Schuh, H. (2006). Global mapping function (GMF): A new empirical mapping function based on numerical weather model data. *Geophysical Research Letters*, 33(7), L07304. <https://doi.org/10.1029/2005GL025546>
- Costantino, G., Giffard-Roisin, S., Marsan, D., Marill, L., Radiguet, M., Dalla Mura, M., et al. (2022). Seismic source characterization from GNSS data using deep learning. *Journal of Geophysical Research: Solid Earth*, 128(4), e2022JB024930. <https://doi.org/10.1029/2022jb024930>
- Costantino, G., Giffard-Roisin, S., Radiguet, M., Dalla Mura, M., Marsan, D., & Socquet, A. (2023). Slow slip detection with deep learning in multi-station raw geodetic time series validated against tremors in cascadia. *arXiv preprint arXiv:2305.19720*. Communications Earth 'I and' Environment. <https://doi.org/10.48550/arXiv.2305.19720>
- Delahaye, E., Townend, J., Reyners, M., & Rogers, G. (2009). Microseismicity but no tremor accompanying slow slip in the Hikurangi subduction zone, New Zealand. *Earth and Planetary Science Letters*, 277(1–2), 21–28. <https://doi.org/10.1016/j.epsl.2008.09.038>
- Dragert, H., Wang, K., & James, T. S. (2001). A silent slip event on the deeper cascadia subduction interface. *Science*, 292(5521), 1525–1528. <https://doi.org/10.1126/science.1060152>
- El Yousfi, Z., Radiguet, M., Rousset, B., Husker, A., Kazachkina, E., & Kostoglodov, V. (2023). Intermittence of transient slow slip in the Mexican subduction zone. *Earth and Planetary Science Letters*, 620, 118340. <https://doi.org/10.1016/j.epsl.2023.118340>
- Farrell, W. E. (1972). Deformation of the Earth by surface loads. *Reviews of Geophysics*, 10(3), 761–797. <https://doi.org/10.1029/RG010i003p00761>
- Frank, W. B., & Brodsky, E. E. (2019). Daily measurement of slow slip from low-frequency earthquakes is consistent with ordinary earthquake scaling. *Science Advances*, 5(10), eaaw9386. <https://doi.org/10.1126/sciadv.aaw9386>
- Frank, W. B., Radiguet, M., Rousset, B., Shapiro, N. M., Husker, A. L., Kostoglodov, V., et al. (2015). Uncovering the geodetic signature of silent slip through repeating earthquakes. *Geophysical Research Letters*, 42(8), 2774–2779. <https://doi.org/10.1002/2015GL063685>
- Frank, W. B., Rousset, B., Lasserre, C., & Campillo, M. (2018). Revealing the cluster of slow transients behind a large slow slip event. *Science Advances*, 4(5), eaat0661. <https://doi.org/10.1126/sciadv.aat0661>
- Fukuda, J. (2018). Variability of the space-time evolution of slow slip events off the Boso Peninsula, Central Japan, from 1996 to 2014. *Journal of Geophysical Research: Solid Earth*, 123(1), 732–760. <https://doi.org/10.1002/2017JB014709>
- Gardonio, B., Campillo, M., Marsan, D., Lecointre, A., Bouchon, M., & Letort, J. (2019). Seismic activity preceding the 2011 Mw9.0 Tohoku earthquake, Japan, analyzed with multidimensional template matching. *Journal of Geophysical Research: Solid Earth*, 124(7), 6815–6831. <https://doi.org/10.1029/2018JB016751>
- Gardonio, B., Marsan, D., Bouchon, M., Socquet, A., Jara, J., Sun, Q., et al. (2018). Revisiting slow slip events occurrence in Boso Peninsula, Japan, combining GPS data and repeating earthquakes analysis. *Journal of Geophysical Research: Solid Earth*, 123(2), 1502–1515. <https://doi.org/10.1002/2017JB014469>
- Gomberg, J., Wech, A., Creager, K., Obara, K., & Agnew, D. (2016). Reconsidering earthquake scaling. *Geophysical Research Letters*, 43(12), 6243–6251. <https://doi.org/10.1002/2016gl069967>
- Hanks, T. C., & Kanamori, H. (1979). A moment magnitude scale. *Journal of Geophysical Research*, 84(B5), 2348–2350. <https://doi.org/10.1029/JB084iB05p02348>
- Hasegawa, A., & Yoshida, K. (2015). Preceding seismic activity and slow slip events in the source area of the 2011 Mw 9.0 Tohoku-Oki earthquake: A review. *Geoscience Letters*, 2(1), 6. <https://doi.org/10.1186/s40562-015-0025-0>

- Hayes, G. P., Moore, G. L., Portner, D. E., Hearne, M., Flamme, H., Furtney, M., & Smoczyk, G. M. (2018). Slab2, a comprehensive subduction zone geometry model. *Science*, 362(6410), 58–61. <https://doi.org/10.1126/science.aat4723>
- Heki, K., & Mitsui, Y. (2013). Accelerated Pacific plate subduction following interplate thrust earthquakes at the Japan Trench. *Earth and Planetary Science Letters*, 363, 44–49. <https://doi.org/10.1016/j.epsl.2012.12.031>
- Heki, K., Miyazaki, S., & Tsuji, H. (1997). Silent fault slip following an interplate thrust earthquake at the Japan Trench. *Nature*, 386(6625), 595–598. <https://doi.org/10.1038/386595a0>
- Hirose, H., Kimura, H., Enescu, B., & Aoi, S. (2012). Recurrent slow slip event likely hastened by the 2011 Tohoku earthquake. *Proceedings of the National Academy of Sciences*, 109(38), 15157–15161. <https://doi.org/10.1073/pnas.1202709109>
- Hooper, A., Pietrzak, J., Simons, W., Cui, H., Riva, R., Naeije, M., et al. (2013). Importance of horizontal seafloor motion on tsunami height for the 2011 Mw=9.0 Tohoku-Oki earthquake. *Earth and Planetary Science Letters*, 361, 469–479. <https://doi.org/10.1016/j.epsl.2012.11.013>
- Ide, S., & Beroza, G. C. (2023). Slow earthquake scaling reconsidered as a boundary between distinct modes of rupture propagation. *Proceedings of the National Academy of Sciences*, 120(32), e2222102120. <https://doi.org/10.1073/pnas.2222102120>
- Ide, S., Beroza, G. C., Shelly, D. R., & Uchida, T. (2007). A scaling law for slow earthquakes. *Nature*, 447(7140), 76–79. <https://doi.org/10.1038/nature05780>
- Imanishi, K., Ando, R., & Kuwahara, Y. (2012). Unusual shallow normal-faulting earthquake sequence in compressional northeast Japan activated after the 2011 off the Pacific coast of Tohoku earthquake. *Geophysical Research Letters*, 39(9), L09306. <https://doi.org/10.1029/2012GL051491>
- Ita, A., Tonegawa, T., Uchida, N., Yamamoto, Y., Suetsugu, D., Hino, R., et al. (2019). Configuration and structure of the Philippine Sea plate off Boso, Japan: Constraints on the shallow subduction kinematics, seismicity, and slow slip events. *Earth Planets and Space*, 71(1), 111. <https://doi.org/10.1186/s40623-019-1090-y>
- Ito, Y., Hino, R., Kido, M., Fujimoto, H., Osada, Y., Inazu, D., et al. (2013). Episodic slow slip events in the Japan subduction zone before the 2011 Tohoku-Oki earthquake. *Tectonophysics*, 600, 14–26. <https://doi.org/10.1016/j.tecto.2012.08.022>
- Kato, A., Obara, K., Igarashi, T., Tsuruoka, H., Nakagawa, S., & Hirata, N. (2012). Propagation of slow slip leading up to the 2011 Mw 9.0 Tohoku-oki earthquake. *Science*, 335(6069), 705–708. <https://doi.org/10.1126/science.1215141>
- Khoshramesh, M., Shirzaei, M., & Uchida, N. (2020). Deep slow-slip events promote seismicity in northeastern Japan megathrust. *Earth and Planetary Science Letters*, 540, 116261. <https://doi.org/10.1016/j.epsl.2020.116261>
- Klein, E., Duputel, Z., Zigone, D., Vigny, C., Boy, J.-P., Doubre, C., & Meneses, G. (2018). Deep transient slow slip detected by survey GPS in the region of Atacama, Chile. *Geophysical Research Letters*, 45(22), 12–263. <https://doi.org/10.1029/2018gl080613>
- Kobayashi, A. (2017). Objective detection of long-term slow slip events along the Nankai Trough using GNSS data (1996–2016). *Earth Planets and Space*, 69(1), 171. <https://doi.org/10.1186/s40623-017-0755-7>
- Loveless, J. P., & Meade, B. J. (2016). Two decades of spatiotemporal variations in subduction zone coupling offshore Japan. *Earth and Planetary Science Letters*, 436, 19–30. <https://doi.org/10.1016/j.epsl.2015.12.033>
- Lowry, A. R., Larson, K. M., Kostoglodov, V., & Bilham, R. (2001). Transient fault slip in Guerrero, southern Mexico. *Geophysical Research Letters*, 28(19), 3753–3756. <https://doi.org/10.1029/2001GL013238>
- Lyard, F. H., Allain, D. J., Cancet, M., Carrère, L., & Picot, N. (2021). FES2014 global ocean tide atlas: Design and performance. *Ocean Science*, 17(3), 615–649. <https://doi.org/10.5194/os-17-615-2021>
- Marill, L., Marsan, D., Rousset, B., & Socquet, A. (2024). Geodetic matched filter slow slip event detection along the northern Japan subduction zones. [Dataset]. <https://www.gsi.go.jp/english/geonetenglish.html>
- Marill, L., Marsan, D., Socquet, A., Radiguet, M., Cotte, N., & Rousset, B. (2021). Fourteen-year acceleration along the Japan trench. *Journal of Geophysical Research: Solid Earth*, 126(11), e2020JB021226. <https://doi.org/10.1029/2020JB021226>
- Marsan, D., Bouchon, M., Gardonio, B., Perfettini, H., Socquet, A., & Enescu, B. (2017). Change in seismicity along the Japan Trench, 1990–2011, and its relationship with seismic coupling. *Journal of Geophysical Research: Solid Earth*, 122(6), 4645–4659. <https://doi.org/10.1002/2016JB013715>
- Marsan, D., Reverso, T., Helmstetter, A., & Enescu, B. (2013). Slow slip and aseismic deformation episodes associated with the subducting Pacific plate offshore Japan, revealed by changes in seismicity. *Journal of Geophysical Research: Solid Earth*, 118(9), 4900–4909. <https://doi.org/10.1002/jgrb.50323>
- Mavrommatis, A. P., Segall, P., & Johnson, K. M. (2014). A decadal-scale deformation transient prior to the 2011 Mw 9.0 Tohoku-oki earthquake. *Geophysical Research Letters*, 41(13), 4486–4494. <https://doi.org/10.1002/2014GL060139>
- Mavrommatis, A. P., Segall, P., Uchida, N., & Johnson, K. M. (2015). Long-term acceleration of aseismic slip preceding the Mw 9 Tohoku-oki earthquake: Constraints from repeating earthquakes. *Geophysical Research Letters*, 42(22), 9717–9725. <https://doi.org/10.1002/2015GL066069>
- Michel, S., Gualandi, A., & Avouac, J.-P. (2019a). Interseismic coupling and slow slip events on the Cascadia megathrust. *Pure and Applied Geophysics*, 176(9), 3867–3891. <https://doi.org/10.1007/s00024-018-1991-x>
- Michel, S., Gualandi, A., & Avouac, J.-P. (2019b). Similar scaling laws for earthquakes and Cascadia slow-slip events. *Nature*, 574(7779), 522–526. <https://doi.org/10.1038/s41586-019-1673-6>
- NIED S-net. (2019). National Research Institute for Earth Science and Disaster Resilience, NIED S-net. <https://doi.org/10.17598/nied.0007>
- Nishikawa, T., & Ide, S. (2017). Detection of earthquake swarms at subduction zones globally: Insights into tectonic controls on swarm activity: Detection of Earthquake Swarms. *Journal of Geophysical Research: Solid Earth*, 122(7), 5325–5343. <https://doi.org/10.1002/2017JB014188>
- Nishikawa, T., Matsuzawa, T., Ohta, K., Uchida, N., Nishimura, T., & Ide, S. (2019). The slow earthquake spectrum in the Japan Trench illuminated by the S-net seafloor observatories. *Science*, 365(6455), 808–813. <https://doi.org/10.1126/science.aax5618>
- Nishikawa, T., Nishimura, T., & Okada, Y. (2021). Earthquake swarm detection along the Hikurangi trench, New Zealand: Insights into the relationship between seismicity and slow slip events. *Journal of Geophysical Research: Solid Earth*, 126(4), e2020JB020618. <https://doi.org/10.1029/2020JB020618>
- Nishimura, T. (2021). Slow slip events in the Kanto and Tokai regions of Central Japan detected using global navigation satellite system data during 1994–2020. *Geochemistry, Geophysics, Geosystems*, 22(2), e2020GC009329. <https://doi.org/10.1029/2020GC009329>
- Nishimura, T., Matsuzawa, T., & Obara, K. (2013). Detection of short-term slow slip events along the Nankai Trough, southwest Japan, using GNSS data. *Journal of Geophysical Research: Solid Earth*, 118(6), 3112–3125. <https://doi.org/10.1002/jgrb.50222>
- Nishimura, T., Sagiya, T., & Stein, R. S. (2007). Crustal block kinematics and seismic potential of the northernmost Philippine Sea plate and Izu microplate, central Japan, inferred from GPS and leveling data. *Journal of Geophysical Research*, 112(B5), B05414. <https://doi.org/10.1029/2005JB004102>
- Okada, Y. (1985). Surface deformation due to shear and tensile faults in a half-space. *Bulletin of the Seismological Society of America*, 75(4), 1135–1154. [https://doi.org/10.1016/0148-9062\(86\)90674-1](https://doi.org/10.1016/0148-9062(86)90674-1)

- Okada, Y., Nishimura, T., Tabei, T., Matsushima, T., & Hirose, H. (2022). Development of a detection method for short-term slow slip events using GNSS data and its application to the nankai subduction zone. *Earth Planets and Space*, 74(1), 1–18. <https://doi.org/10.1186/s40623-022-01576-8>
- Ozawa, S., Murakami, M., & Tada, T. (2001). Time-dependent inversion study of the slow thrust event in the Nankai trough subduction zone, southwestern Japan. *Journal of Geophysical Research*, 106(B1), 787–802. <https://doi.org/10.1029/2000JB900317>
- Ozawa, S., Suito, H., & Tobita, M. (2007). Occurrence of quasi-periodic slow-slip off the east coast of the Boso peninsula, Central Japan. *Earth Planets and Space*, 59(12), 1241–1245. <https://doi.org/10.1186/BF03352672>
- Ozawa, S., Yarai, H., & Kobayashi, T. (2019). Recovery of the recurrence interval of Boso slow slip events in Japan. *Earth Planets and Space*, 71(1), 78. <https://doi.org/10.1186/s40623-019-1058-y>
- Passarelli, L., Selvadurai, P. A., Rivalta, E., & Jónsson, S. (2021). The source scaling and seismic productivity of slow slip transients. *Science Advances*, 7(32), eabg9718. <https://doi.org/10.1126/sciadv.abg9718>
- Peltzer, G., Rosen, P., Rogez, F., & Hudnut, K. (1996). Postseismic rebound in fault step-overs caused by pore fluid flow. *Science*, 273(5279), 1202–1204. <https://doi.org/10.1126/science.273.5279.1202>
- Peng, Z., & Gombert, J. (2010). An integrated perspective of the continuum between earthquakes and slow-slip phenomena. *Nature Geoscience*, 3(9), 599–607. <https://doi.org/10.1038/ngeo940>
- Perfettini, H., & Avouac, J. (2014). The seismic cycle in the area of the 2011 Mw9.0 Tohoku-Oki earthquake. *Journal of Geophysical Research: Solid Earth*, 119(5), 4469–4515. <https://doi.org/10.1002/2013JB010697>
- Priollat, A., Radiguet, M., Weiss, J., Twardzik, C., Amtrano, D., Cotte, N., et al. (2022). Transient brittle creep mechanism explains early postseismic phase of the 2011 Tohoku-oki megathrust earthquake: Observations by high-rates GPS solutions. *Earth and Space Science Open Archive*, 127(8), e2022JB024005. <https://doi.org/10.1002/essoar.10510262.1>
- Radiguet, M., Cotton, F., Vergnolle, M., Campillo, M., Walpersdorf, A., Cotte, N., & Kostoglodov, V. (2012). Slow slip events and strain accumulation in the Guerrero gap, Mexico. *Journal of Geophysical Research*, 117(B4), B04305. <https://doi.org/10.1029/2011JB008801>
- Rousset, B., Bürgmann, R., & Campillo, M. (2019). Slow slip events in the roots of the San Andreas Fault. *Science Advances*, 5(2), eaav3274. <https://doi.org/10.1126/sciadv.aav3274>
- Rousset, B., Campillo, M., Lasserre, C., Frank, W. B., Cotte, N., Walpersdorf, A., et al. (2017). A geodetic matched filter search for slow slip with application to the Mexico subduction zone. *Journal of Geophysical Research: Solid Earth*, 122(12), 10–498. <https://doi.org/10.1002/2017JB014448>
- Rousset, B., Fu, Y., Bartlow, N., & Bürgmann, R. (2019). Weeks-long and years-long slow slip and tectonic tremor episodes on the south central Alaska megathrust. *Journal of Geophysical Research: Solid Earth*, 124(12), 13392–13403. <https://doi.org/10.1029/2019JB018724>
- Schmidt, D., & Gao, H. (2010). Source parameters and time-dependent slip distributions of slow slip events on the cascadia subduction zone from 1998 to 2008. *Journal of Geophysical Research*, 115(B4). <https://doi.org/10.1029/2008jb006045>
- Scholz, C. H., & Campos, J. (2012). The seismic coupling of subduction zones revisited. *Journal of Geophysical Research*, 117(B5). <https://doi.org/10.1029/2011jb009003>
- Schreiber, T., & Schmitz, A. (1996). Improved surrogate data for nonlinearity tests. *Physical Review Letters*, 77(4), 635–638. <https://doi.org/10.1103/physrevlett.77.635>
- Socquet, A., Marill, L., Deschamps-Huygen, G., & Janex, G. (2022). GNSS daily position solutions in Japan. CNRS, OSUG, ISTERRE. https://doi.org/10.17178/GNSS.PRODUCTS.JAPAN_GIPSYX.DAILY
- Sun, T., & Wang, K. (2015). Viscoelastic relaxation following subduction earthquakes and its effects on afterslip determination. *Journal of Geophysical Research: Solid Earth*, 120(2), 1329–1344. <https://doi.org/10.1002/2014JB011707>
- Sun, T., Wang, K., Inuma, T., Hino, R., He, J., Fujimoto, H., et al. (2014). Prevalence of viscoelastic relaxation after the 2011 Tohoku-Oki earthquake. *Nature*, 514(7520), 84–87. <https://doi.org/10.1038/nature13778>
- Takagi, R., Uchida, N., & Obara, K. (2019). Along-strike variation and migration of long-term slow slip events in the western nankai subduction zone, Japan. *Journal of Geophysical Research: Solid Earth*, 124(4), 3853–3880. <https://doi.org/10.1029/2018JB016738>
- Uchida, N., Inuma, T., Nadeau, R. M., Bürgmann, R., & Hino, R. (2016). Periodic slow slip triggers megathrust zone earthquakes in northeastern Japan. *Science*, 351(6272), 488–492. <https://doi.org/10.1126/science.aad3108>
- Uchida, N., Matsuzawa, T., Nakajima, J., & Hasegawa, A. (2010). Subduction of a wedge-shaped Philippine Sea plate beneath Kanto, central Japan, estimated from converted waves and small repeating earthquakes. *Journal of Geophysical Research*, 115(B7), B07309. <https://doi.org/10.1029/2009JB006962>
- Wallace, L. M., & Beavan, J. (2010). Diverse slow slip behavior at the Hikurangi subduction margin, New Zealand. *Journal of Geophysical Research*, 115(B12). <https://doi.org/10.1029/2010jb007717>
- Yokota, Y., & Koketsu, K. (2015). A very long-term transient event preceding the 2011 Tohoku earthquake. *Nature Communications*, 6(1), 5934. <https://doi.org/10.1038/ncomms6934>